

Generalized Solution for Double-Porosity Flow through a Graded Excavation Damaged Zone

Kristopher L. Kuhlman¹

¹Sandia National Laboratories, Nuclear Waste Disposal Research & Analysis, PO Box 5800, Mail Stop 0747, Albuquerque NM, 87185, USA.

Contributing authors: klkuhlm@sandia.gov;

Abstract

Prediction of flow to boreholes or excavations in fractured low-permeability rocks is important for resource extraction and disposal or sequestration activities. Analytical solutions for fluid pressure and flowrate, when available, are powerful, insightful, and efficient tools enabling parameter estimation and uncertainty quantification. A flexible porous media flow solution for arbitrary physical dimension is derived and extended to double porosity for converging radial flow when permeability and porosity decrease radially as a power law away from a borehole or opening. This distribution can arise from damage accumulation due to stress relief associated with drilling or mining. The single-porosity graded conductivity solution was initially found for heat conduction, the arbitrary dimension flow solution comes from hydrology, and the solution with both arbitrary dimension and graded permeability distribution appeared in reservoir engineering. These existing solutions are here combined and extended to two implementations of the double-porosity conceptual model, for both a simpler thin-film mass transfer and more physically realistic diffusion between fracture and matrix. This work presents a new specified-flowrate solution with wellbore storage for the simpler double-porosity model, and a new more physically realistic solution for any wellbore boundary condition. A new closed-form expression is derived for the matrix diffusion solution (applicable to both homogeneous and graded problems), improving on previous infinite series expressions.

Keywords: double porosity, excavation damaged zone, porous media flow, fractured rock, salt, analytical solution

1 Introduction

Fluid flow through damage-induced fracture networks in otherwise low-permeability crystalline rocks (e.g., granite, argillite or halite) is of interest to geothermal energy production (Tao et al, 2021), radioactive waste disposal (Tsang et al, 2005), hydrogen storage (AbuAisha and Billiotte, 2021), and compressed air energy storage (Kim et al, 2012). Rock damage around an excavation (i.e., the Excavation Damaged Zone, EDZ; Davies and Bernier (2005)) increases the connected porosity, and leads to increased permeability. Fractured rock often has higher porosity and permeability than intact rock. Damage near a borehole or excavation will decrease the relative contribution from flow in the lower-permeability far-field, and will confound the estimation of hydrologic properties using approaches that assume uniform homogeneous distributions of permeability and porosity. There is a need for a flexible analytical solution for flow to a borehole or excavation in the presence of damage, that includes wellbore storage, double-porosity flow, and variable flow dimension. This is most evident in a mechanically weak, low-permeability medium like salt, but should also apply to other low-permeability fractured rocks like granite or shale.

In salt, the far-field (i.e., undamaged) permeability is unmeasurably low (Beauheim and Roberts, 2002) due to salt's tendency to creep shut any unsupported openings. The permeability around a borehole in salt is derived from accumulated damage due to stress redistribution around the excavation itself (Wallace et al, 1990; Stormont et al, 1991; Cosenza, 1996; Hou, 2003; Kuhlman, 2014).

Stormont et al (1991) presented brine and gas permeability data measured in salt for packer-isolated intervals of small boreholes before and after a central 1-meter diameter borehole was drilled (i.e., a mine-by experiment). Figure 1 shows these data support the conceptual model of permeability and porosity decaying away from an excavation. Cosenza (1996) proposed the power-law model for permeability and porosity plotted in the figure. These data show porosity and permeability decrease with distance from the central excavation. Two lines are shown with to the data; one is a monomial power-law, the other includes an additive background term. The two curves differ primarily away from the excavation ($r/r_w \geq 3$), where larger uncertainties in estimated porosity and permeability exist, for three reasons. First, the access drift EDZ (test conducted in the floor of a 5-m wide room) is superimposed on the 1-m borehole EDZ. Second, the small-diameter (2.5-cm) measurement boreholes themselves each have a small EDZ overprinted on the 1-m borehole EDZ. Lastly, the apparent background permeability may represent the measurement limit of the packer system used (i.e., compliance of the packer inflation elements and working fluid). Especially in salt, the undisturbed background permeability is near zero, and is difficult to measure consistently in the field (Beauheim and Roberts, 2002). The power-law distribution of permeability matches the more certain near-field permeability distribution, and is conceptually more elegant than a finite domain or a flow domain with piece-wise heterogeneous properties (i.e., a higher-permeability EDZ adjacent to lower-permeability intact rock). Other investigations have also shown porosity and permeability decaying away with distance from an excavation in crystalline rocks (Shen et al, 2011; Cho et al, 2013; Ghazvinian, 2015) and sedimentary rocks (Perras et al, 2010; Perras and Diederichs, 2016).

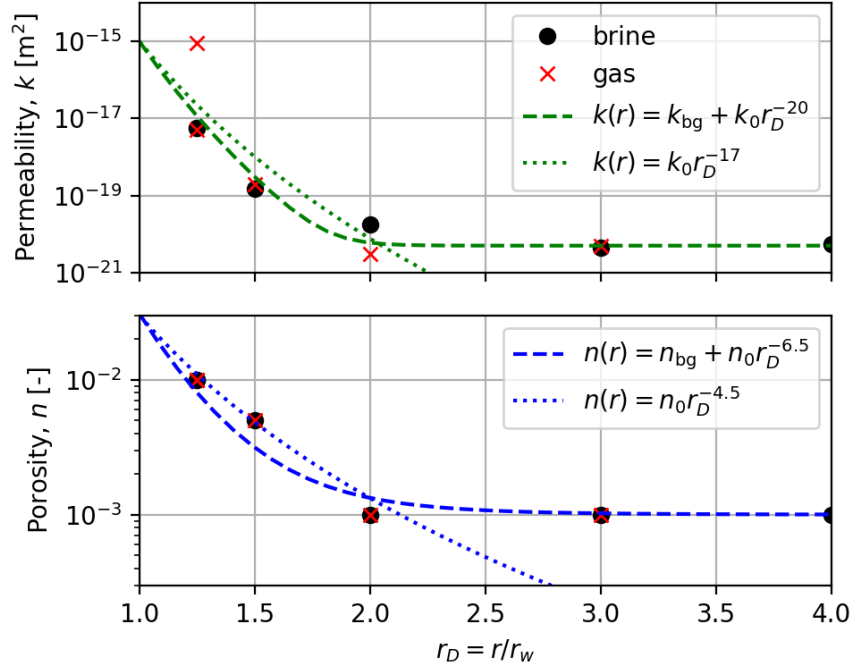


Fig. 1 Permeability and porosity observations around a 1-m borehole (radial distance scaled by excavation radius) in salt from small-scale mine-by experiment (data from Stormont et al (1991))

Salt permeability has been related to both the confining and shear stresses (Reynolds and Gloyna, 1960; Lai, 1971; Stormont and Fuenkajorn, 1994; Alkan, 2009). Confining stresses reduce fracture aperture and bulk permeability, while shear stresses are associated with increased bulk permeability. Aydan et al (1993) present solutions for radial and tangential plane stress and strain (i.e., dilatation or a change in porosity) around a circular excavation. Strain is proportional to r_D^{-2} or r_D^{-3} (where r_D is radial distance

into the formation scaled by the excavation size), depending on whether the region is experiencing elastic (exponent 2) or plastic (exponent ≈ 3) deformation. These relationships illustrate a possible behavior of rock in the EDZ. The true extent of the EDZ depends on drilling or excavation method, borehole or tunnel geometry, state of stress, and rock mechanical properties (Hudson et al, 2009). Softer or weaker sedimentary rocks like argillite or halite typically have a larger EDZ than stiffer or stronger rocks like granite.

There are several well-known empirical power-law relationships between porosity and permeability in fractured or granular media (e.g., Kozeny, 1927; Carman, 1937) and many studies have discussed their applicability (David et al, 1994; Kuhlman and Matteo, 2018). Permeability in fractured rocks is more sensitive to small changes in porosity than granular rocks (i.e., fractured rocks have higher pore compressibility resulting in larger exponents in porosity-permeability relationships).

Based on evidence from these observations, graded dimensionless porosity is assumed to follow

$$n(r) = n_0 \left(\frac{r}{r_w} \right)^{-\eta}, \quad (1)$$

where r_w is the borehole or excavation radius [m], $n_0 = n(r_w)$ is maximum porosity at the borehole wall, and η is a dimensionless exponent (see Table 1 for a list of physical variables and notation). Using the same form, the graded permeability can be represented with the form

$$k(r) = k_0 \left(\frac{r}{r_w} \right)^{-\kappa}, \quad (2)$$

where $k_0 = k(r_w)$ is the maximum permeability [m^2] at the borehole wall and κ is another dimensionless exponent. Based on lab measurements on fractured granite, the empirical relationship $\kappa \approx 3\eta$ has been proposed (Kranz et al, 1979; David et al, 1994). The Stormont et al (1991) salt data (Figure 1) support $\eta = 4.5$ and $\kappa = 17$, which shows a somewhat faster-decaying permeability ($\kappa = 3.8\eta$) than seen in granitic rocks.

The power-law permeability and porosity distribution conceptual model presented here is an alternative to flow models using wellbore skin (Streletsova, 1988; Pasandi et al, 2008), finite domain (Gelbard, 1992; Lin et al, 2016), or low-permeability non-Darcy flow with a threshold gradient (Liu, 2014, 2017). These three conceptualizations all lead to reduced contributions of flow from the far field, but only borehole skin can account for observed distributions of higher porosity or permeability near the excavation, which are important when analyzing pressure or flowrate data at early time. The contribution from lower permeability in the far field are more important at late time. Finite domains and skin can have analytical flow solutions, but low-permeability non-Darcy flow does not typically lend itself to analytical solutions.

Barker (1988) developed a generalized solution for converging flow to a borehole with variable non-integer dimension, D . This conceptualization has been used to characterize flow in fractured systems, where lower-dimension (i.e., $D < 3$) results associated with discrete fractures are more common than higher dimension results (Beauheim et al, 2004; Le Borgne et al, 2004; Bowman et al, 2013; Ferroud et al, 2018). Doe (1991) extended the solution of Barker (1988) to the conceptualization where permeability varies with radial distance, through analogy with the heat conduction literature (Carslaw and Jaeger, 1959).

A single-porosity flow solution is derived here with power-law variable properties, like the approach of Doe (1991) (who did not present a derivation). The single-porosity solution is then readily extended to a double-porosity conceptualization, using first the approach of Warren and Root (1963) for thin-film mass transfer between fractures and matrix, then the more physically realistic matrix diffusion approach of Kazemi (1969).

Double-porosity flow is a common and efficient conceptualization in fractured rocks (Aguilera, 1980; van Golf-Racht, 1982; Da Prat, 1990). The medium is conceptualized as two communicating physically overlapping continua including fractures with high permeability (but little to no storage) and matrix or intact rock with significant storage (but little to no flow) (Barenblatt and Zheltov, 1960; Barenblatt et al, 1960). Many extensions to the basic double-porosity conceptual model exist, including multiple matrix or fracture porosities, and different assumptions about the geometry or underlying physics governing flow in the fractures or matrix (Chen, 1989; Kuhlman and Heath, 2021). The Warren and Root (1963)

solution simplifies the exchange between matrix and fractures to a mass-transfer thin-film approximation, leading to numerous analytical solutions (Aguilera, 1980; Chen, 1989). It is commonly used for this reason, even though it is well-known that spatial pressure gradients in matrix blocks are important, as the matrix is low-permeability and would therefore be expected to experience steep, slow-changing gradients. A series representation of the Kazemi (1969) solution is used here, an extension of the multirate mass transfer model to double-porosity flow (Kuhlman et al, 2015). The more physically correct (but more difficult to solve) solution can be represented by an infinite series of porosities, which can either represent an infinite number of Warren-Root type matrix porosities, or if the coefficients are chosen specifically, a single Kazemi-type matrix diffusion porosity. More recently, Wang et al (2021) has developed a semi-analytical solution for flow in a double-porosity formation, for the case when non-Darcian flow is significant. Moutsopoulos et al (2022) have provided analytical and semi-analytical solutions for two classical problems in flow of unconfined double-porosity aquifers, based on Moutsopoulos (2021). De-Smedt (2022) presented an analytical solution for flow in double-porosity media for fractional flow dimensions, which is a generalization of De-Smedt (2011). Hayek et al (2018) presented a semi-analytical solution for flow due to pumping a double-porosity aquifer via a constant-pressure boundary condition (without wellbore storage) where permeability varied as a power law.

The fractal reservoir flow problem (Chang and Yortsos, 1990) is also analogous to the radially variable properties approach presented here, but the governing equations of the two problems are only equivalent when the spectral exponent (θ in Chang and Yortsos (1990)) in the fractal problem is zero. The fractal reservoir governing equation is typically solved approximately, since the additional terms due to non-zero spectral exponent in the governing equation do not readily allow closed-form analytical solution.

In the next section, the governing equations and boundary conditions are developed for the variable-dimension single-porosity flow problem (Doe, 1991). This solution is mapped onto the modified Bessel equation, allowing solution for flow to both specified pressure (type-I) and specified flowrate with wellbore storage (type-III). These more general single-porosity solutions are shown to degenerate down to several well-known cases. The single-porosity solutions are then extended to a simpler Warren-Root type double-porosity model for type-I (Hayek et al, 2018) and type-III (new) and then a new Kazemi type double-porosity model. The Kazemi series solution approach is then summed analytically to arrive at a new closed-form expression for the response in Laplace space, a solution that is new for both graded and homogeneous domains. Finally, a summary and discussion of limitations is given for the new solutions.

The approach taken here, representing the porosity and permeability of fractured rocks as power-law distributions, was first developed by Delay et al (2007), and first pursued by the author for applications in deep (> 3 km) borehole disposal of radioactive waste in basement rock (Brady et al, 2017; Kuhlman et al, 2019). The approach is also applicable to flow in salt surrounding excavations, like those in mine-by experiments (Stormont et al, 1991).

2 Development of Flow Problem

To introduce and contrast with the dual-porosity solution, the single-porosity solution is developed first. To make a single solution for Cartesian linear, cylindrical, and spherical geometries, a variable-dimension approach like Barker (1988) is used, including variable permeability and porosity, like Doe (1991). The governing equation for slightly compressible time-dependent change in pressure p [Pa] in a general 1D coordinate (Barker, 1988) is

$$n(r)c \frac{\partial p}{\partial t} = \frac{1}{r^m} \frac{\partial}{\partial r} \left[\frac{k(r)r^m}{\mu} \frac{\partial p}{\partial r} \right], \quad (3)$$

where c is bulk compressibility [1/Pa] and the dimensionless parameter m is 0 for a Cartesian strip, 1 for a cylinder, and 2 for a sphere (i.e., $m = D - 1$, where D is the dimension). The derivative of the bracketed term in (3) is expanded via chain rule; starting from (2), $\frac{dk}{dr} = -\kappa k(r)/r$ is substituted with the definitions of $k(r)$ and $n(r)$, to get

$$n_0 c \left(\frac{r}{r_w} \right)^{-\eta} \frac{\partial p}{\partial t} = \frac{k_0}{\mu} \left(\frac{r}{r_w} \right)^{-\kappa} \left[\frac{m - \kappa}{r} \frac{\partial p}{\partial r} + \frac{\partial^2 p}{\partial r^2} \right]. \quad (4)$$

For converging radial flow in a semi-infinite domain, the relevant wellbore boundary conditions are constant-pressure (type-I), constant-flux (type-II), or constant-flux with wellbore storage (type-III in

Laplace space). The initial, far-field, and source borehole boundary conditions for a borehole in an infinite symmetric domain are

$$\begin{aligned}
& \text{initial} \quad p(r, t = 0) = 0 \\
& \text{far - field} \quad p(r \rightarrow \infty, t) < \infty \\
& \text{wellbore type - I} \quad p^I(r = r_w, t) = p_1(t); \quad \text{or} \\
& \text{wellbore type - II} \quad \left. \frac{A_m k_0}{\mu} \frac{\partial p^{II}(t)}{\partial r} \right|_{r=r_w} = Q(t); \quad \text{or} \\
& \text{wellbore type - III} \quad \left. \frac{A_m k_0}{\mu} \frac{\partial p^{III}(t)}{\partial r} \right|_{r=r_w} = Q(t) + \frac{A_c}{\rho g} \frac{\partial p_w(t)}{\partial t},
\end{aligned} \tag{5}$$

respectively. See Appendix A for definition of source borehole boundary condition terms. These boundary conditions represent a homogeneous uniform initial condition, a requirement that the solution remains finite at large distance, and a specified pressure or pressure gradient at the source ($r = r_w$).

The Type-II boundary condition (specified flowrate) is a special case ($\sigma = 0$) of the wellbore storage boundary condition (flowrate linearly proportional to change in pressure), so it is not developed further.

2.1 Dimensional Analysis

A solution is derived for equation (4), using the approach of Doe (1991), which was based on analogy with the heat conduction literature (Carslaw and Jaeger, 1959). Reducing the governing equation (4) to dimensionless form using characteristic time, $T_c = n_0 c L_c^2 \mu / k_0$, and characteristic length, $L_c = r_w$, leads to

$$r_D^{\kappa-\eta} \frac{\partial p_D}{\partial t_D} = \frac{m - \kappa}{r_D} \frac{\partial p_D}{\partial r_D} + \frac{\partial^2 p_D}{\partial r_D^2}, \tag{6}$$

where the dimensionless quantities $r_D = r/L_c$, $t_D = t/T_c$, and $p_D^{\{I, III\}} = p/p_c^{\{I, III\}}$ are used (see Table 2 for a summary of dimensionless quantities).

The characteristic pressure change is given by $p_c^I = \hat{p}_1$, where $p_1(t) = \hat{p}_1 f_t$ separates the time-dependent specified pressure into a constant characteristic pressure and a dimensionless variable time behavior (for a constant specified pressure, $f_t = 1$). The dimensionless type-I initial and boundary conditions are

$$\begin{aligned}
p_D(r_D, t_D = 0) &= 0 \\
p_D(r_D \rightarrow \infty, t_D) &< \infty \\
p_D^I(r_D = 1, t_D) &= f_t.
\end{aligned} \tag{7}$$

Using $p_c^{III} = \frac{r_w \hat{Q} \mu}{A_m k_0}$, where $Q(t) = \hat{Q} f_t$ similarly separates the time-dependent volumetric flowrate into a constant characteristic flowrate and a dimensionless time behavior. The dimensionless type-III source borehole boundary condition is

$$\left. \frac{\partial p_D^{III}}{\partial r_D} \right|_{r_D=1} = f_t + \sigma \frac{\partial p_D^{III}}{\partial t}, \tag{8}$$

where σ is a dimensionless wellbore storage coefficient (see Appendix A) and the same initial and far-field conditions apply as the type-I case.

2.2 Laplace Transform

Taking the dimensionless Laplace transform ($\bar{f}(s) = \int_0^\infty e^{-st_D} f(t_D) dt_D$) of the governing partial differential equation (6) (without loss of generality assuming zero initial condition) leads to the ordinary differential equation

$$\frac{d^2 \bar{p}_D}{dr_D^2} + \frac{m - \kappa}{r_D} \frac{d\bar{p}_D}{dr_D} - s \bar{p}_D r_D^{\kappa-\eta} = 0, \tag{9}$$

assuming κ , η , and m are not functions of time, and s is the dimensionless Laplace transform parameter.

The transformed type-I and far-field boundary conditions (7) are

$$\begin{aligned}\bar{p}_D(r_D \rightarrow \infty) &< \infty \\ \bar{p}_D^I(r_D = 1) &= \bar{f}_t,\end{aligned}\tag{10}$$

where \bar{f}_t represents the Laplace transform of the boundary condition's time behavior. For a unit step change at $t = 0$ (where $f_t = 1$, a typical assumption), $\bar{f}_t = \frac{1}{s}$. Other temporal behaviors are simply handled, including a step change at a non-zero time, an exponentially decaying source term, an arbitrary piecewise-constant or piecewise-linear behavior, or a sinusoidal source term (Kruseman and de Ridder, 1994; Mishra et al, 2013).

The transformed wellbore-storage boundary condition is

$$\left. \frac{d\bar{p}_D^{III}}{dr_D} \right|_{r_D=1} = \bar{f}_t + \sigma s \bar{p}_D^{III},\tag{11}$$

which now more clearly resembles a Type-III boundary condition.

2.3 Numerical Inverse Laplace Transform

The governing equations and associated boundary conditions are solved exactly in Laplace space, then numerically inverted back to the time domain using one of several viable approaches (Kuhlman, 2013). The equations were rapidly prototyped and inverted using the Python library mpmath (Johansson et al, 2017), which provides arbitrary precision special functions and numerical inverse Laplace transform algorithms. A Fortran program was also developed to facilitate plotting and parameter estimation, implementing the inversion algorithm of de Hoog et al (1982). Python and Fortran implementations of the solution are available at <https://github.com/klkuhlm/graded>.

3 Solution of Flow Problem

3.1 Mapping onto Modified Bessel Equation

The governing ordinary differential equation (9) can be made equivalent to a form of the modified Bessel equation after a change of variables first used by Lommel (1868) for the standard Bessel equation. Appendix B illustrates an analogous change of variables to the modified Bessel equation. Comparing (9) to this scaled version of the modified Bessel equation (41), they are equivalent given the following correspondences

$$\begin{aligned}\alpha &= \frac{1}{2}(\kappa - m + 1) & \gamma &= \frac{1}{2}(\kappa - \eta + 2) \\ \nu &= \sqrt{\frac{\alpha^2}{\gamma^2}} = \frac{\kappa - m + 1}{\kappa - \eta + 2} & \beta &= \sqrt{\frac{s}{\gamma^2}} = \sqrt{\frac{4s}{(\kappa - \eta + 2)^2}}.\end{aligned}\tag{12}$$

The transformed modified Bessel equation has the general solution (37)

$$y = z^\alpha [AI_\nu(\beta z^\gamma) + BK_\nu(\beta z^\gamma)], \quad (\gamma \neq 0),\tag{13}$$

where A and B are constants determined by the boundary conditions and $I_\nu(z)$ and $K_\nu(z)$ are the first- and second-kind modified Bessel functions of non-integer order and real argument (McLachlan, 1955; Bowman, 1958; Spanier and Oldham, 1987; DLMF, 2023).

The finiteness boundary condition (10) requires $A = 0$ to keep the solution finite as $r_D \rightarrow \infty$, since the first-kind modified Bessel function grows exponentially with increasing real argument, leaving

$$\bar{p}_D(r_D) = r_D^\alpha BK_\nu(\beta r_D^\gamma),\tag{14}$$

which is not defined for $\gamma = 0$ (i.e., $\kappa - \eta = -2$, which is unrealistic because κ is larger than η for physical reasons), and B is determined by the Laplace-space source borehole boundary conditions.

3.2 Constant-Pressure (Type-I) at Borehole

The borehole boundary condition ($r_D = 1$) for specified change in pressure leads to the solution (the Warren and Root (1963) double porosity solution for this wellbore boundary condition is equivalent to Hayek et al (2018))

$$\bar{p}_D^I(r_D) = \bar{f}_t r_D^\alpha \frac{K_\nu(\beta r_D^\gamma)}{K_\nu(\beta)} \quad (15)$$

and its radial gradient (i.e., proportional to flow of fluid into the borehole)

$$\frac{d\bar{p}_D^I}{dr_D} = \bar{f}_t r_D^{\alpha-1} \left[(\alpha - \gamma\nu) \frac{K_\nu(\beta r_D^\gamma)}{K_\nu(\beta)} + \beta\gamma r_D^\gamma \frac{K_{\nu-1}(\beta r_D^\gamma)}{K_\nu(\beta)} \right], \quad (16)$$

using a recurrence relationship for the derivative of the Bessel function in terms of Bessel functions of adjacent orders (DLMF, 2023, §10.29.2).

Restricting $\kappa \geq \eta$ (i.e., permeability decreases as fast or faster than porosity), then $\gamma > 0$ and $\alpha = \gamma\nu$ (for $\gamma < 0$, $\alpha - \gamma\nu = 2\alpha$). This physically motivated restriction on parameters simplifies (16) to

$$\frac{d\bar{p}_D^I}{dr_D} = \sqrt{s} \bar{f}_t r_D^{\alpha+\gamma-1} \frac{K_{\nu-1}(\beta r_D^\gamma)}{K_\nu(\beta)}, \quad (17)$$

since $\beta\gamma = \sqrt{s}$ for $\gamma > 0$. When evaluated in the source borehole ($r_D = 1$), the solution simplifies further.

Figure 2 shows plots of the predicted pressure gradient at $r_D = 1$ due to a constant-pressure condition there (top row) and the predicted decrease in pressure radially away from the boundary (values of η , κ , and m for each simulation are listed in the caption and title of each figure). Both rows of plots show the variability with the porosity exponent (η , given by the line color) and the permeability exponent ($\kappa = \eta\tau$, given by the line type). The same results are shown for Cartesian linear ($m = 0$), cylindrical ($m = 1$), and spherical ($m = 2$) geometries in three columns.

For a given set of parameters, a higher-dimensional domain (larger m) leads to a slower drop in produced fluids at any time. The highest sustained flowrate for all dimensions is achieved with constant properties in space (i.e., the red curve $\eta = \kappa = 0$). More negative exponents in the porosity and permeability power-laws lead to more rapid decrease in flowrate, as the contribution to flow from large radius vanishes when the exponent increases in magnitude. These types of responses might be mis-interpreted as being associated with lower permeability (which would also lead to a faster decrease in flowrate) using a model with constant properties and a fixed dimension.

In the source well (top row of subplots), the effect of κ is different and are predicted to reverse between dimensions. For $\eta = 3$ (black lines), the $\kappa = \{3, 6, 9\}$ cases are swapped between $m = 1$ and $m = 2$. For $\eta = 2$ (blue lines), the κ cases are swapped between $m = 0$ and $m = 1$.

The bottom row of figures shows the predicted pressure with distance at $t_D = 10$. At locations away from the source well ($r_D > 1$), changes in the porosity exponent, η , have relatively less impact than changes in the permeability exponent, κ (different colored solid lines are close together, while colored lines of different line type are widely separated). The dimensionality (m) has a smaller effect at locations away from the source borehole than it had on the gradient predicted at the source borehole.

3.3 Constant-Flowrate with Wellbore Storage (Type-III)

The wellbore-storage boundary condition for the specified flowrate solution at $r_D = 1$ results in the general solution (that is new for any double-porosity solution with power-law variation in material properties)

$$\bar{p}_D^{III}(r_D) = \bar{f}_t r_D^\alpha \frac{K_\nu(\beta r_D^\gamma)}{(\alpha - \gamma\nu + \sigma s) K_\nu(\beta) + \beta\gamma K_{\nu-1}(\beta)}, \quad (18)$$

which can be simplified using $\alpha = \gamma\nu$ and $\beta\gamma = \sqrt{s}$ to

$$\bar{p}_D^{III}(r_D) = \bar{f}_t r_D^\alpha \frac{K_\nu(\beta r_D^\gamma)}{\sqrt{s} K_{\nu-1}(\beta) + \sigma s K_\nu(\beta)}. \quad (19)$$

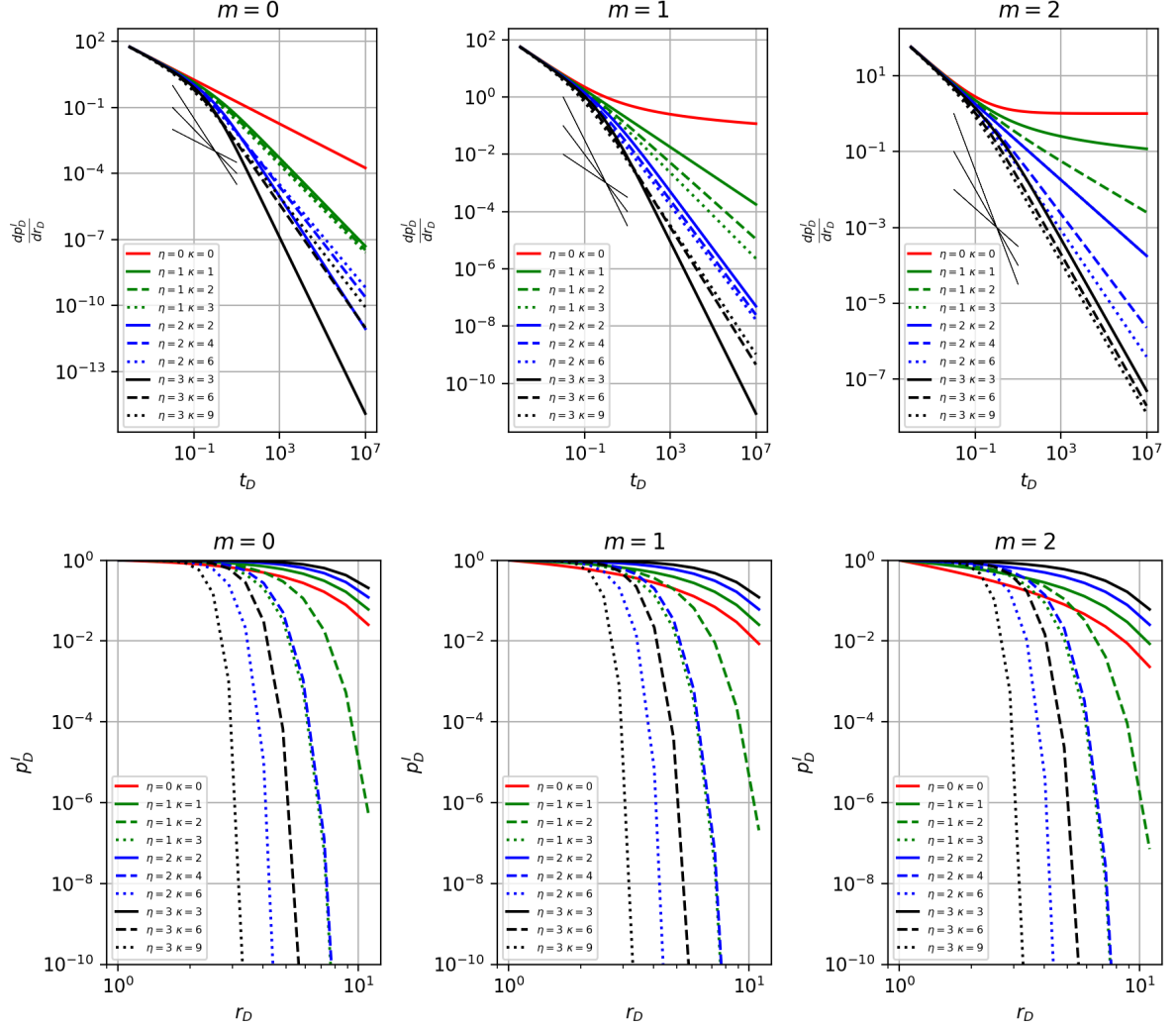


Fig. 2 Type-I flowrate (top row at $r_D = 1$) and pressure (bottom row at $r_D > 1$ and $t_D = 10$) solution at borehole for $m = 0, 1, 2$ (Cartesian, cylindrical, and spherical) and at different radial distances. Line color indicates η ; line type indicates κ/η . Line segments in top row illustrate slopes of $1/2$, 1 , and $3/2$.

Analogous to the results for the Type-I solution but only showing the $m = 1$ and $m = 2$ cases, Figure 3 shows the predicted pressure through time at the boundary for a specified flowrate at the boundary. Figure 3 results are for no wellbore storage ($\sigma = 0$), while Figure 4 shows the same results with non-zero wellbore storage (all model parameters listed in caption or title of each figure). Wellbore storage is important at early time, leading to a smaller predicted change in pressure, with the predicted response giving a characteristic $1 : 1$ slope on log-log plots before formation storage contributes significantly to the flow (i.e., pumping in a bathtub). Wellbore storage makes more of a difference (i.e., shows a larger deviation from $\sigma = 0$ case) for larger η (and κ , since $\kappa = 2\eta$).

3.4 Parameter Combinations Yielding Simpler Solutions

When $\eta = \kappa = 0$, permeability and porosity are constant in space; in this case (9) simplifies to

$$\frac{d^2 \bar{p}_D}{dr_D^2} + \frac{m}{r_D} \frac{d\bar{p}_D}{dr_D} - s\bar{p}_D = 0, \quad (20)$$

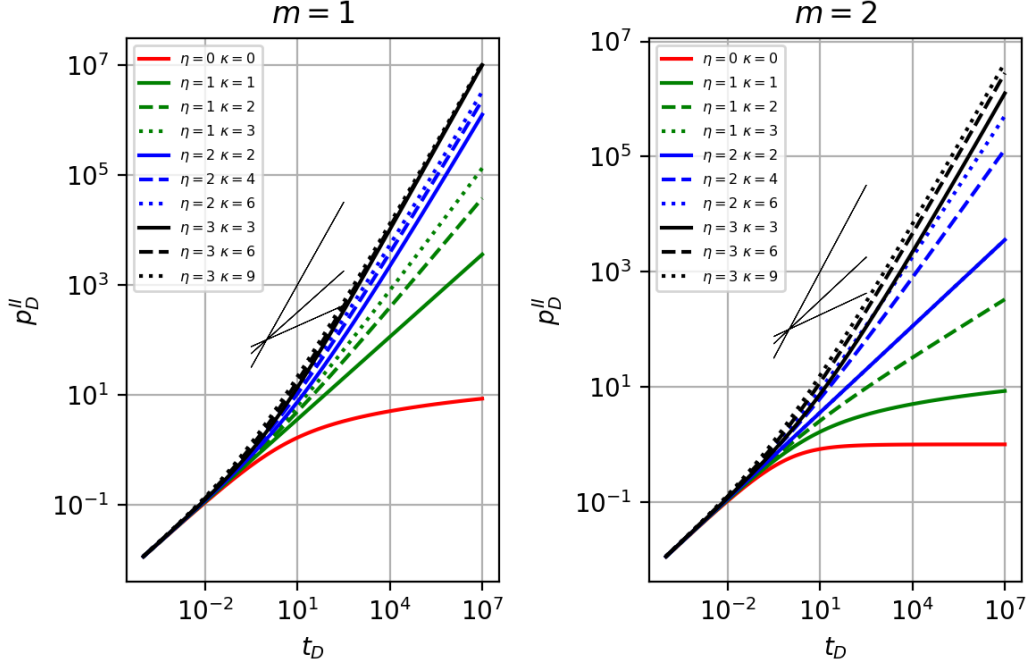


Fig. 3 Type-II solution (Type-III with $\sigma = 0$) at borehole for $m = 1, 2$ (cylindrical and spherical). Line color indicates η ; line type indicates κ/η .

which is the dimensionless form of the equation solved by [Barker \(1988\)](#). In this case $\gamma = 1$, $\alpha = (1-m)/2$, $\nu = \alpha$, and $\beta = \sqrt{s}$. The solution in Laplace-space under these conditions becomes

$$\bar{p}_D(r_D) = r_D^\nu B K_\nu(\sqrt{s} r_D), \quad (21)$$

which was found by [Barker \(1988, Eqn. 15\)](#).

When $\eta = \kappa = m = 0$ the time-domain solution simplifies to $p_D(t) = 1/\sqrt{\pi t}$, because $\nu = 1/2$ and $\nu - 1 = -1/2$, the numerator and denominator of (17) are equal since $K_\nu(z) \equiv K_{-\nu}(z)$.

Another simplification occurs when $m = \kappa = \eta$, not necessarily zero. In this case, the permeability and porosity decrease at the same rate radially that the surface area of the domain grows in size ($A_0 \propto 1$, $A_1 \propto r_D$, $A_2 \propto r_D^2$), resulting in an equivalent Cartesian coordinate system,

$$\frac{d^2 \bar{p}_D}{dr_D^2} - s \bar{p}_D = 0, \quad (22)$$

which has a solution in terms of $\sin(\sqrt{s} r_D)$ and $\cos(\sqrt{s} r_D)$ or $\exp(\pm \sqrt{s} r_D)$ and typically has an explicit inverse Laplace transform. In this case $\alpha = \nu = 1/2$, $\gamma = 0$, and $\beta = \sqrt{s}$.

When $\nu = n \pm \frac{1}{2}$ (for n integer), the modified Bessel functions become modified spherical Bessel functions ([DLMF, 2023, §10.47](#)), and when $\nu = \pm \frac{1}{3}$, they become Airy functions ([DLMF, 2023, §9.6](#)). These additional special cases are not handled differently here (i.e., the more general solution in terms of modified Bessel functions is still valid), since in the case given here ν varies with κ , η , and m (12).

4 Extension of Solution to Double Porosity

4.1 Mass-Transfer Coefficient Approximation

Beginning with the [Warren and Root \(1963\)](#) formulation for double-porosity (i.e., high-conductance fractures and high-capacity matrix), the power-law permeability and porosity distributions are incorporated.

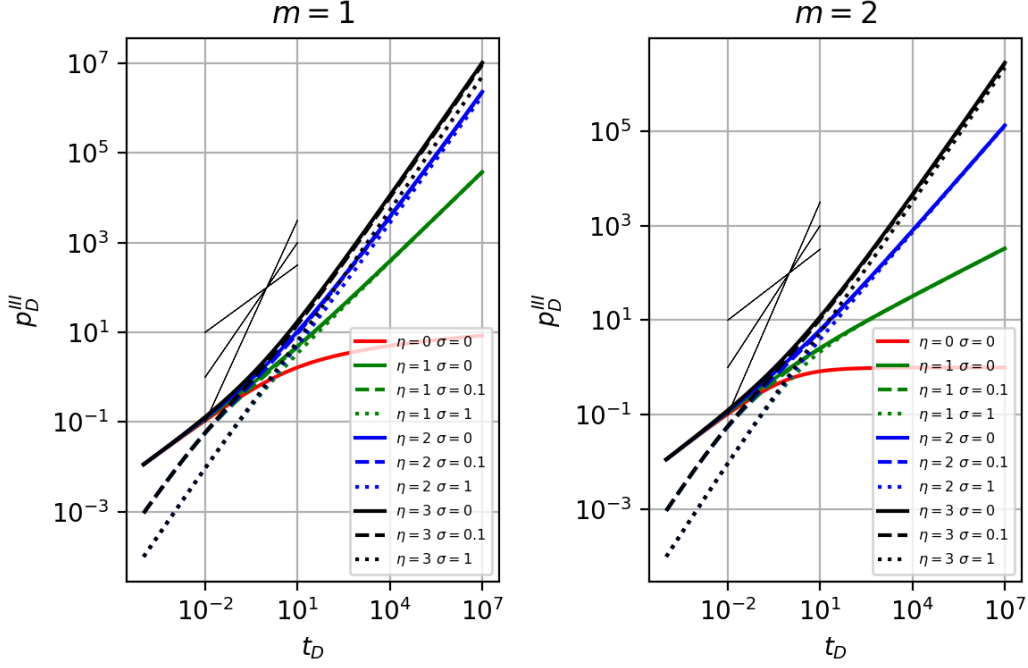


Fig. 4 Type-III solution at borehole ($r_D = 1$), for $m = 1, 2$ (cylindrical and spherical). Line color indicates η ; line type indicates σ . All curves for $\kappa/\eta = 2$.

The equations for double-porosity flow in the fractures and matrix are

$$\begin{aligned} \frac{1}{r^m} \frac{\partial}{\partial r} \left[\frac{k_f}{\mu} \frac{\partial p_f}{\partial r} \right] &= n_r c_r \frac{\partial p_r}{\partial t} + n_f c_f \frac{\partial p_f}{\partial t} \\ \frac{\hat{\alpha} k_r}{\mu} (p_f - p_r) &= n_r c_r \frac{\partial p_r}{\partial t} \end{aligned} \quad (23)$$

where $\hat{\alpha}$ is the shape factor [$1/\text{m}^2$] of Warren and Root (1963), subscript f indicates fracture, and subscript r indicates matrix (rock). The matrix equation does not involve a spatial gradient of pressure, nor a matching of pressure and flux at the boundary, but simply a difference between the fracture and matrix pressure (i.e., the mass transfer coefficient approximation often used for heat transfer across thin films). This behavior is sometimes referred to in the petroleum engineering literature as “steady-state” flow between the fracture and matrix (Da Prat, 1990), but it also represents one-dimensional diffusion in the matrix with a thin-film mass-transfer approximation between the fracture and matrix reservoirs, analogous to Newton’s law of cooling.

Substituting the permeability $k_i = k_{i0} \left(\frac{r}{r_w} \right)^{-\kappa_i}$ and porosity $n_i = n_{i0} \left(\frac{r}{r_w} \right)^{-\eta_i}$ ($i \in \{f, r\}$), then converting to dimensionless form using an analogous approach to Warren and Root (1963), where $\omega = n_{f0} c_f / (n_{r0} c_r + n_{f0} c_f)$ is the dimensionless fracture storage coefficient and $\lambda = \hat{\alpha} k_r r_w^2 / k_f$ is the dimensionless interporosity exchange coefficient. Finally, taking the Laplace transform of both equations results in the pair of ordinary differential equations

$$\begin{aligned} \left[\frac{d^2 \bar{p}_{fD}}{dr_D^2} + \frac{m - \kappa_f}{r_D} \frac{d\bar{p}_{fD}}{dr_D} \right] r^{-\kappa_f} &= (1 - \omega) r_D^{-\eta_r} \bar{p}_{mD} s + \omega r_D^{-\eta_f} \bar{p}_{fD} s \\ \lambda (\bar{p}_{fD} - \bar{p}_{rD}) r_D^{-\kappa_r} &= (1 - \omega) r_D^{-\eta_r} \bar{p}_{rD} s. \end{aligned} \quad (24)$$

Solving for matrix pressure in the matrix equation, $\bar{p}_{rD} = \bar{p}_{fD} \lambda r_D^{-\kappa_r} / [(1 - \omega) s r_D^{-\eta_r} + \lambda r_D^{-\kappa_r}]$, and substituting this into the fracture equation leads to a single equation solely in terms of dimensionless

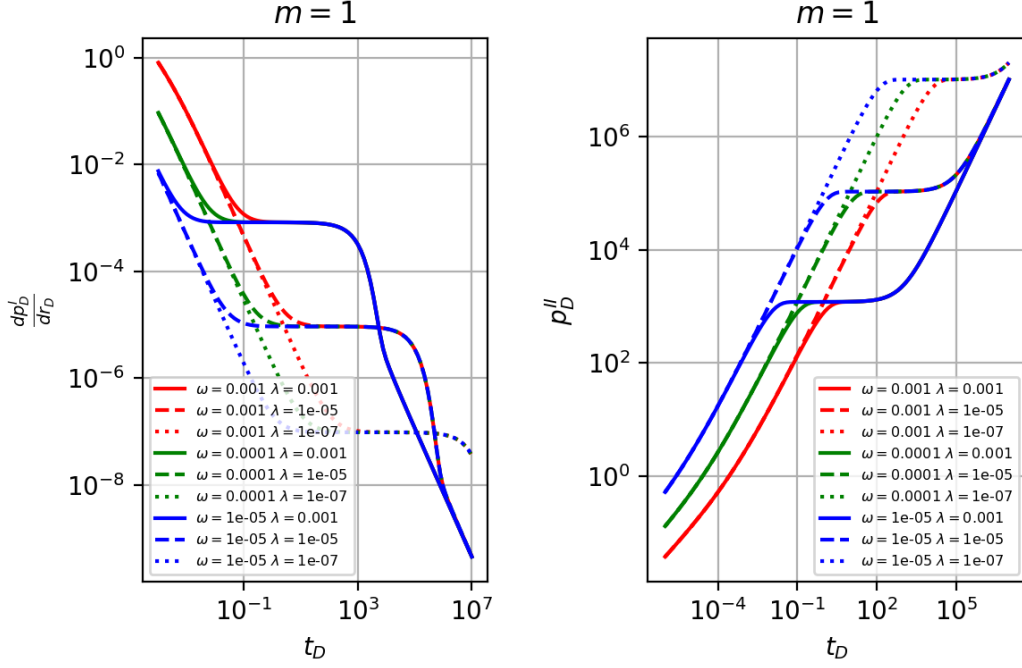


Fig. 5 Type-I flowrate solution at borehole (left) and Type-II solution for pressure ($\sigma = 0$, right), for $m = 1$ (cylindrical). Line color indicates λ ; line type indicates ω .

Laplace-domain fracture pressure

$$\left[\frac{d^2 \bar{p}_{fD}}{dr_D^2} + \frac{m - \kappa_f}{r_D} \frac{d\bar{p}_{fD}}{dr_D} \right] r^{-\kappa_f} = r_D^{-\eta_r} \bar{p}_{fD} \left\{ \frac{(1 - \omega) s r_D^{-\kappa_r} \lambda}{(1 - \omega) s r_D^{-\eta_r} + \lambda r_D^{-\kappa_r}} \right\} + \omega r_D^{-\eta_f} \bar{p}_{fD} s. \quad (25)$$

To force the term in curly brackets in (25) to be independent of r_D , $\kappa_r = \eta_r$ is assumed. Setting κ_r and η_r equal to η_f allows r_D and \bar{p}_{fD} to be similar form to previous solutions. Simplifying the subsequent notation $\kappa_f \rightarrow \kappa$, $\eta_r \rightarrow \eta$, and $\bar{p}_{fD} \rightarrow \bar{p}_D$ results in

$$\frac{d^2 \bar{p}_D}{dr_D^2} + \frac{m - \kappa}{r_D} \frac{d\bar{p}_D}{dr_D} = r_D^{\kappa - \eta} \bar{p}_D \left[\frac{(1 - \omega) s \lambda}{(1 - \omega) s + \lambda} + \omega s \right], \quad (26)$$

which is the same form as (9). This solution corresponds to the same scaled Bessel equation, with only the definition of β changing to

$$\beta_{WR} = \sqrt{\left[\frac{\lambda}{\lambda/(1 - \omega) + s} + \omega \right] \frac{s}{\gamma^2}}. \quad (27)$$

Any more general spatial behavior of matrix properties (e.g., $\eta_r \neq \kappa_r$) would not be solvable with the same approach. This limitation still makes physical sense, as the the most important terms to vary with space are the fracture permeability and the matrix storage. Setting $\kappa = \eta = 0$ and $m = 1$ results in the Warren and Root (1963) solution.

Figure 5 shows typical solution behaviors for the cylindrical ($m = 1$) case for Type-I and Type-II wellbore boundary conditions, for $\eta = 3$ and $\kappa = 6$. Figure 6 shows behavior from the “middle” curve in Figure 5 ($\lambda = 10^{-5}$ and $\omega = 10^{-4}$), for a range of porosity and permeability exponents similar to those shown in Warren and Root (1963), listed in the figure caption.

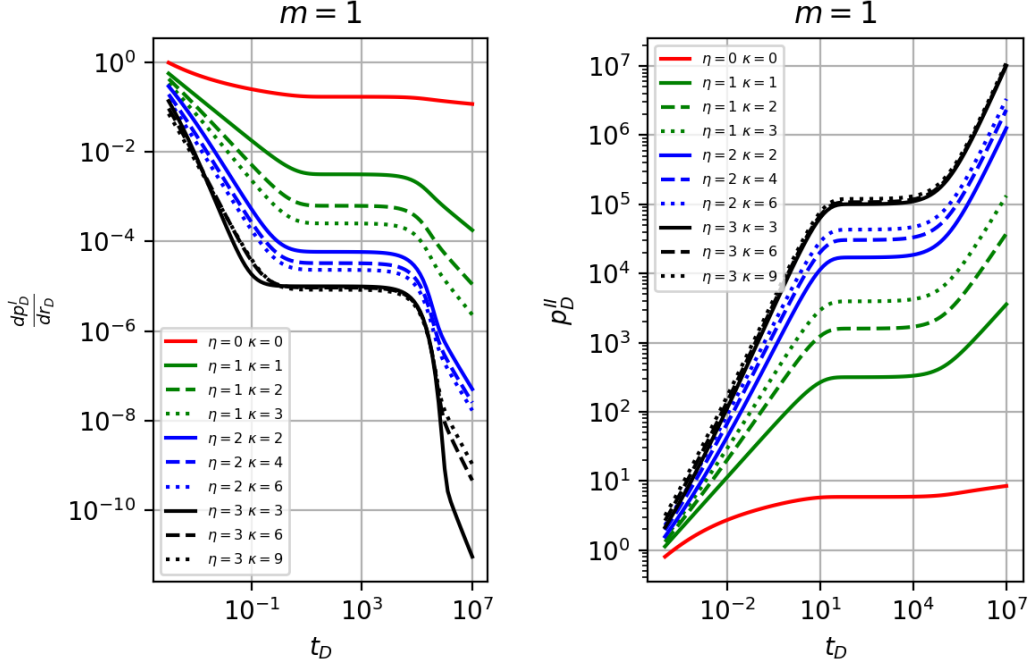


Fig. 6 Type-I flowrate solution at borehole (left) and Type-II solution for pressure ($\sigma = 0$, right), for $m = 1$ (cylindrical). All curves are for $\lambda = 10^{-5}$ and $\omega = 10^{-4}$ (middle curves shown in Figure 5). Line color indicates η ; line type indicates κ/η .

4.2 Matrix Diffusion

The matrix diffusion problem of Kazemi (1969) is more physically realistic (Aguilera, 1980; Da Prat, 1990), but it is typically solved numerically or via late-time approximations (De Swaan, 1976), rather than analytically like Warren and Root (1963). The series approach of Kuhlman et al (2015) is used here to represent matrix diffusion in a single matrix continuum through the sum of an infinite series of Warren-Root matrix continua, and the infinite sum is then analytically summed.

The generalization of (23) to multiple matrix continua starts with

$$\begin{aligned} \frac{1}{r^m} \frac{\partial}{\partial r} \left[\frac{k_f}{\mu} \frac{\partial p_f}{\partial r} \right] &= \sum_{j=1}^N n_j c_j \frac{\partial p_j}{\partial t} + n_f c_f \frac{\partial p_f}{\partial t} \\ \frac{\hat{\alpha}_j k_j}{\mu} (p_f - p_j) &= n_j c_j \frac{\partial p_j}{\partial t} \quad j = 1, 2, \dots, N, \end{aligned} \quad (28)$$

where N is the number of matrix continua (one additional equation for each continuum). Similarly taking the Laplace transform of this set of equations, solving for \bar{p}_f , substituting the matrix equations into the fracture equation, and simplifying the notation leads to

$$\frac{d^2 \bar{p}_D}{dr_D^2} + \frac{m - \kappa}{r_D} \frac{d\bar{p}_D}{dr_D} = r_D^{\kappa - \eta} \bar{p}_D \omega s (1 + \bar{g}), \quad (29)$$

where

$$\bar{g} = \sum_{j=1}^N \frac{\hat{\xi}_j u_j}{s + u_j} \quad (30)$$

is a matrix memory kernel (Haggerty and Gorelick, 1995), $\hat{\xi}_j$ is related to the storage properties of each matrix continuum (analogous to ω of Warren and Root (1963)), and u_j is related to the interporosity flow coefficient of each matrix continuum (analogous to λ of Warren and Root (1963)). The Laplace-space memory kernel approach is flexible, and is used elsewhere in hydrology and reservoir engineering (Herrera and Yates, 1977; Haggerty et al, 2000; Schumer et al, 2003). Equation (29) can be simplified to

Warren and Root (1963) with a particular choice of \bar{g} and $N = 1$, and to the solution for a triple-porosity reservoir (Clossman, 1975) with a different choice of \bar{g} and $N = 2$ (Kuhlman et al, 2015).

When $N \rightarrow \infty$ in (30), it is more convenient to specify the mean and variance of the parameter distributions than the individual parameters associated with each porosity. Several different distributions are possible (Haggerty and Gorelick, 1995). In the form presented by Kuhlman et al (2015), the parameters are specified as the infinite series

$$u_j = \frac{(2j-1)^2 \pi^2 \lambda}{4(1-\omega)} \quad \hat{\xi}_j = \frac{8(1-\omega)}{(2j-1)^2 \omega \pi^2} \quad j = 1, 2, \dots, N \rightarrow \infty \quad (31)$$

which leads to the Kazemi (1969) solution for matrix diffusion. The parameters λ and ω have the same definitions as in Warren and Root (1963).

Setting $\kappa = \eta = 0$ results in the solution of Kuhlman et al (2015). The new governing equation is the same form and the modified Bessel function solution, only requiring re-definition of β as

$$\beta_{KZ} = \sqrt{\left[\sum_{j=1}^N \frac{\omega \hat{\xi}_j u_j}{u_j + s} + \omega \right] \frac{s}{\gamma^2}}, \quad N \rightarrow \infty. \quad (32)$$

Substituting the definitions of u and $\hat{\xi}$ from (31) and simplifying leads to

$$\beta_{KZ} = \sqrt{\left[\sum_{j=1}^N \frac{2\lambda}{W_j^2 \lambda / (1-\omega) + s} + \omega \right] \frac{s}{\gamma^2}}, \quad N \rightarrow \infty, \quad (33)$$

where $W_j = \pi(2j-1)/2$. This is similar in form to (27) but the term in the denominator grows as the index increases, illustrating how the series solution approximates the Kazemi (1969) solution through an infinite series of modified Warren and Root (1963) matrix porosities.

Further simplifying the approach of Kuhlman et al (2015), the infinite series in (33) can be evaluated in closed form using residue methods (Wolfram Research, Inc., 2021), resulting in

$$\beta_{KZ} = \sqrt{\left[\sqrt{\frac{\lambda(1-\omega)}{s}} \tanh\left(\sqrt{\frac{s(1-\omega)}{\lambda}}\right) + \omega \right] \frac{s}{\gamma^2}}, \quad (34)$$

where $\tanh(\cdot)$ is the hyperbolic tangent. This closed-form expression derived here is more accurate and numerically more efficient than truncating or accelerating the infinite series in (32), which is an improvement over the series presented in Kuhlman et al (2015) for graded or homogeneous domains.

Figure 7 illustrates the transition from the Warren and Root (1963) ($N = 1$) to the Kazemi (1969) series approximation for increasing terms ($N = \{2, 10, 100, 1000\}$, heavy colored solid lines) and the expression for the infinite sum (34) (heavy black dashed line) for flow to a specified flux (type-II, $\sigma = 0$) cylindrical ($m = 1$) borehole of constant material properties ($\kappa = \eta = 0$). The bounding Theis (1935) behavior is shown for the fracture and matrix compressibilities (thin red dashed lines).

5 Applications and Limitations

A general converging radial flow solution for specified flowrate or specified wellhead pressure was derived for domains with power-law variability in porosity and permeability due to damage. The single-porosity version has already been presented by Doe (1991), and a solution for constant-pressure condition without wellbore storage was derived by Hayek et al (2018), but the specified-flowrate double-porosity solution with wellbore storage presented here is new. The infinite series approximation to Kazemi was summed analytically, resulting in a new closed-form expression of the series presented in Kuhlman et al (2015), which is an improvement for both graded and homogeneous properties. The newly developed analytical solutions are more general (i.e., several existing solutions are special cases of the new solution) and include more behaviors typical in well-test solutions (i.e., wellbore storage, positive skin, double porosity),

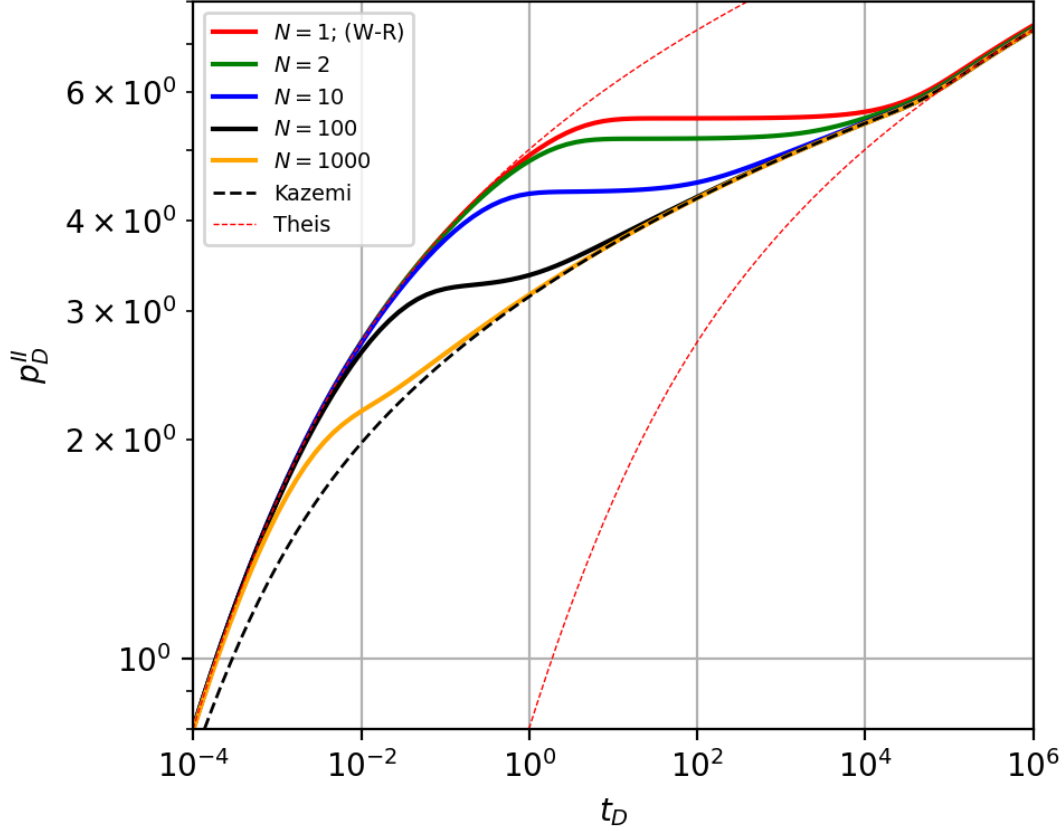


Fig. 7 Type-II solution for pressure at source borehole ($\sigma = 0$), for $m = 1$ (cylindrical) for different number of terms. All curves are for $\lambda = 10^{-5}$, $\omega = 10^{-4}$, $\kappa = \eta = 0$.

while still being straightforward and parsimonious (i.e., as few free parameters as possible) in their implementation.

The basic flow solution assumes linear single-phase flow of a fluid in a slightly compressible formation. The double-porosity solution assumes the fractures are high permeability, with low storage capacity, while the matrix (i.e., intact rock between fractures) is high storage capacity with low permeability. These assumptions are representative for analytical solutions to subsurface porous media flow problems in the hydrology and petroleum engineering literature, and are shared by the solutions of [Barker \(1988\)](#), [Doe \(1991\)](#), [Warren and Root \(1963\)](#), [Kazemi \(1969\)](#), and [Kuhlman et al \(2015\)](#).

To apply this analytical solution to observed data, either observed data would be transformed into dimensionless space, or the analytical solution could be transformed to dimensional space, then a parameter estimation routine would be used to minimize the model-data misfit, and possibly explore the uncertainty or uniqueness of the solution. The solution method developed to solve these solutions uses numerical inverse Laplace transforms and runs quickly enough to be used in parameter estimation (e.g., Monte Carlo methods that require hundreds of thousands of evaluations).

The analytical solution might be of most use with parameter estimation to fit observations, but the non-uniqueness of the curves may make estimation of unique physical parameters difficult, without further physical or site-specific constraints. Realistically, the parameters in the Bessel equation may be estimable (i.e., α , β , γ , and ν defined in (12)), but without defining the flow dimension (m) or the relationship between the porosity and permeability exponents ($\tau = \kappa/\eta$), it may be difficult to identify all the parameters from data alone, since many the curves have similar shapes, unlike classical Type curves ([Bourdet et al, 1989](#)).

A_c	borehole cross-sectional area	m^2
A_m	borehole cylindrical surface area	m^2
c	bulk compressibility	$1/\text{Pa}$
f_t	time variability	—
g	gravitational acceleration	m/s^2
h	hydraulic head	m
k	permeability	m^2
L_c	characteristic length (r_w)	m
m	dimension ($D - 1$)	—
n	porosity	—
p	change in pressure	Pa
s	Laplace transform parameter	—
Q	volumetric flowrate	m^3/s
r	distance coordinate	m
r_w	borehole or excavation radius	m
$\hat{\alpha}$	Warren and Root (1963) shape factor	$1/\text{m}^2$
η	porosity power-law exponent	—
κ	permeability power-law exponent	—
ρ	fluid density	kg/m^3
μ	fluid viscosity	$\text{Pa} \cdot \text{s}$

Table 1 Physical Properties and Parameters

p_D	scaled pressure	p/p_c
t_D	scaled time	$tk_0/n_0cL_c^2\mu$
r_D	scaled distance	r/L_c
λ	interporosity exchange coefficient	$\hat{\alpha}k_r r_w^2/k_f$
σ	wellbore storage coefficient	$A_c/(r_w n_0 c \rho g A_m)$
ω	fracture storage coefficient	$n_{f0}c_f/(n_{r0}c_r + n_{f0}c_f)$

Table 2 Dimensionless Quantities

Statements and Declarations

Funding

The author thanks the U.S. Department of Energy Office of Nuclear Energy’s Spent Fuel and Waste Science and Technology program for funding.

Conflicts of Interest

The author has no competing interests to declare.

Availability of Data and Material

No data or materials were used by the author in the preparation of the manuscript.

Code Availability

The source code of Fortran and Python implementations of the program are available from the author upon request.

Acknowledgments

This paper describes objective technical results and analysis. Any subjective views or opinions that might be expressed in the paper do not necessarily represent the views of the U.S. Department of Energy or the United States Government.

This article has been authored by an employee of National Technology & Engineering Solutions of Sandia, LLC under Contract No. DE-NA0003525 with the U.S. Department of Energy (DOE). The employee owns all right, title and interest in and to the article and is solely responsible for its contents. The United States Government retains and the publisher, by accepting the article for publication, acknowledges that the United States Government retains a non-exclusive, paid-up, irrevocable, world-wide license to publish

or reproduce the published form of this article or allow others to do so, for United States Government purposes. The DOE will provide public access to these results of federally sponsored research in accordance with the DOE Public Access Plan <https://www.energy.gov/downloads/doe-public-access-plan>.

The author thanks Tara LaForce from Sandia for technically reviewing the manuscript.

6 Appendix A: Wellbore Storage Boundary Condition

The wellbore-storage boundary condition accounts for the storage in the finite borehole arising from the mass balance $Q_{\text{in}} - Q_{\text{out}} = A_c \frac{\partial h_w}{\partial t}$. Q_{in} [m^3/s] is volumetric flow into the borehole from the formation, Q_{out} is possibly time-variable flow out of the well through the pump ($Q(t)$ [m^3/s]), and $\frac{\partial h_w}{\partial t}$ is the change in hydraulic head [m] ($h_w = \frac{p_w}{\rho g} + z$) of water standing in the borehole through time, p_w is change in pressure [Pa] of water in the borehole, ρ is fluid density [kg/m^3], z is an elevation datum [m], and g is gravitational acceleration [m/s^2]. A_c is the cross-sectional surface area of the pipe, sphere or box providing storage (it may be a constant or a function of elevation); for a typical pipe, it becomes $A_c = \pi r_c^2$, where r_c is the radius of the casing where the water level is changing. The mass balance is then

$$\frac{A_m k_0}{\mu} \frac{\partial p}{\partial r} \Big|_{r=r_w} - Q(t) = \frac{A_c}{\rho g} \frac{\partial p_w}{\partial t}, \quad (35)$$

where A_m is the area of the borehole communicating with the formation. For the integer m considered here these are $A_0 = b^2$, $A_1 = 2\pi r_w b$, $A_2 = 4\pi r_w^2$ (b is a length independent of the borehole radius).

Assuming the change in water level in the borehole ($h_w = p_w/(\rho g)$) is equal to the change in formation water level ($h = p/(\rho g)$), this can be converted into dimensionless form as

$$\frac{\partial p_D}{\partial r_D} \Big|_{r_D=1} - f_t = \sigma \frac{\partial p_D}{\partial t}, \quad (36)$$

where $\sigma = A_c/(r_w n_0 c \rho g A_m)$ is a dimensionless ratio of formation to wellbore storage; $\sigma \rightarrow 0$ is an infinitesimally small well with only formation response, while $\sigma \rightarrow \infty$ is a well with no formation response (i.e., a bathtub).

7 Appendix B: Transformation of Modified Bessel Equation

Following the approach of Bowman (1958), alternative forms of the Bessel equation are found, this approach is a simplification of the original approach of Lommel (1868). An analogous approach is applied here to “back into” the desired modified Bessel equation. The equation satisfied by the pair of functions

$$y_1 = x^\alpha I_\nu(\beta x^\gamma), \quad y_2 = x^\alpha K_\nu(\beta x^\gamma) \quad (37)$$

is sought, where α , β , γ , and ν are constants. Using the substitutions $\zeta = yx^{-\alpha}$ and $\xi = \beta x^\gamma$ gives $\zeta_1 = I_\nu(\xi)$ and $\zeta_2 = K_\nu(\xi)$, which are the two solutions to the modified Bessel equation (DLMF, 2023, §10.25.1),

$$\xi \frac{d}{d\xi} \left(\xi \frac{d\zeta}{d\xi} \right) - (\xi^2 + \nu)\zeta = 0. \quad (38)$$

Given

$$\xi \frac{d}{d\xi} \left(\xi \frac{d\zeta}{d\xi} \right) = \frac{x}{\gamma^2} \frac{d}{dx} \left(x \frac{d\zeta}{dx} \right), \quad (39)$$

and

$$x \frac{d}{dx} \left(x \frac{d\zeta}{dx} \right) = \frac{y''}{x^{\alpha-2}} - \frac{(2\alpha-1)y'}{x^{\alpha-1}} + \frac{\alpha^2 y}{x^\alpha}, \quad (40)$$

the standard-form equation satisfied by y is

$$y'' + (1 - 2\alpha)y' + \frac{\alpha^2 y}{x^\alpha} - \left(\beta^2 \gamma^2 x^{2\gamma-2} - \frac{\alpha^2 - \nu^2 \gamma^2}{x^2} \right) y = 0. \quad (41)$$

This equation can be compared to the Laplace-space ordinary differential equation (9), allowing direct use of the product of powers and modified Bessel function (37) as solutions (13).

References

- AbuAisha M, Billiotte J (2021) A discussion on hydrogen migration in rock salt for tight underground storage with an insight into a laboratory setup. *Journal of Energy Storage* 38:102958
- Aguilera R (1980) *Naturally Fractured Reservoirs*. PennWell Books
- Alkan H (2009) Percolation model for dilatancy-induced permeability of the excavation damaged zone in rock salt. *International Journal of Rock Mechanics & Mining Sciences* 46(4):716–724
- Aydan Ö, Akagi T, Kawamoto T (1993) The squeezing potential of rocks around tunnels; theory and prediction. *Rock Mechanics and Rock Engineering* 26(2):137–163
- Barenblatt GI, Zheltov YuP (1960) Basic flow equations for homogeneous fluids in naturally fractured rocks. *Doklady Akademii Nauk SSSR* 132(3):545–548
- Barenblatt GI, Zheltov YuP, Kochina IN (1960) Basic concepts in the theory of seepage of homogeneous liquids in fissured rocks [strata]. *Prikladnaya Matematika i Mekhanika* 24(5):852–864
- Barker JA (1988) A generalized radial flow model for hydraulic tests in fractured rock. *Water Resources Research* 24(10):1796–1804
- Beauheim RL, Roberts RM (2002) Hydrology and hydraulic properties of a bedded evaporite formation. *Journal of Hydrology* 259(1):66–88
- Beauheim RL, Roberts RM, Avis JD (2004) Well testing in fractured media: Flow dimension and diagnostic plots. *Journal of Hydraulic Research* 42:69–76
- Bourdet D, Ayoub JA, Pirard YM (1989) Use of pressure derivative in well-test interpretation. *SPE Formation Evaluation* 4(2):293–302
- Bowman DO, Roberts RM, Holt RM (2013) Generalized radial flow in synthetic flow systems. *Groundwater* 51(5):768–774
- Bowman F (1958) *Introduction to Bessel Functions*. Dover
- Brady PV, Freeze GA, Kuhlman KL, et al (2017) Deep borehole disposal of nuclear waste: US perspective. In: *Geological Repository Systems for Safe Disposal of Spent Nuclear Fuels and Radioactive Waste*. Elsevier, p 89–112
- Carman PC (1937) Fluid flow through granular beds. *Transactions of the Institution of Chemical Engineers* 15:150–167
- Carslaw HS, Jaeger JC (1959) *Conduction of Heat in Solids*, 2nd edn. Oxford
- Chang J, Yortsos YC (1990) Pressure-transient analysis of fractured reservoirs. *SPE Formation Evaluation* 5(1):31–38
- Chen ZX (1989) Transient flow of slightly compressible fluids through double-porosity, double-permeability systems – a state-of-the-art review. *Transport in Porous Media* 4(2):147–184
- Cho WJ, Kim JS, Lee C, et al (2013) Gas permeability in the excavation damaged zone at KURT. *Engineering Geology* 164(17):222–229
- Clossman PJ (1975) An aquifer model for fissured reservoirs. *Society of Petroleum Engineers Journal* 15:385–398

- Cosenza Ph (1996) Coupled effects between mechanical behavior and mass transfer phenomena in rock salt. PhD thesis, Ecole Polytechnique
- Da Prat G (1990) Well Test Analysis for Fractured Reservoir Evaluation. No. 27 in Developments in Petroleum Science, Elsevier
- David C, Wong TF, Zhu W, et al (1994) Laboratory measurement of compaction-induced permeability change in porous rocks: Implications for the generation and maintenance of pore pressure excess in the crust. *PAGEOPH* 143(1/2/3):425–456
- Davies C, Bernier F (eds) (2005) Impact of the Excavation Disturbed or Damaged Zone (EDZ) on the Performance of Radioactive Waste Geological Repositories, EUR 21028 EN, Brussels, Belgium
- de Hoog FR, Knight JH, Stokes AN (1982) An improved method for numerical inversion of Laplace transforms. *SIAM Journal of Scientific and Statistical Computing* 3(3):357–366
- De-Smedt F (2011) Analytical solution for constant-rate pumping test in fissured porous media with double-porosity behavior. *Transport in Porous Media* 88:479–489
- De-Smedt F (2022) Analytical solution for fractional well flow in a double-porosity aquifer with fraction transient exchange between matrix and fractures. *Water* 14(456)
- De Swaan AO (1976) Analytic solutions for determining naturally fractured reservoir properties by well testing. *Society of Petroleum Engineers Journal* 16(03):117–122
- Delay F, Kaczmaryk A, Ackerer P (2007) Inversion of interference hydraulic pumping tests in both homogeneous and fractal dual media. *Advances in Water Resources* 30:314–334
- DLMF (2023) *NIST Digital Library of Mathematical Functions*. <http://dlmf.nist.gov/>, Release 1.1.12 of 2023-12-15, URL <http://dlmf.nist.gov/>, f. W. J. Olver, A. B. Olde Daalhuis, D. W. Lozier, B. I. Schneider, R. F. Boisvert, C. W. Clark, B. R. Miller, B. V. Saunders, H. S. Cohl, and M. A. McClain, eds.
- Doe TW (1991) Fractional dimension analysis of constant-pressure well tests. In: SPE Annual Technical Conference and Exhibition, pp 461–467
- Ferroud A, Chesnaux R, Rafini S (2018) Insights on pumping well interpretation from flow dimension analysis: The learnings of a multi-context field database. *Journal of Hydrology* 556:449–474
- Gelbard F (1992) Exact analysis of a two-dimensional model for brine flow to a borehole in a disturbed rock zone. Tech. Rep. SAND92–1303, Sandia National Laboratories, Albuquerque, NM
- Ghazvinian E (2015) Fracture initiation and propagation in low porosity crystalline rocks: Implications for excavation damage zone (EDZ) mechanics. PhD thesis, Queen’s University, Kingston, Ontario, Canada
- van Golf-Racht TD (1982) Fundamentals of Fractured Reservoir Engineering. No. 12 in Developments in Petroleum Science, Elsevier
- Haggerty R, Gorelick SM (1995) Multiple-rate mass-transfer for modeling diffusion and surface-reactions in media with pore-scale heterogeneity. *Water Resources Research* 31(10):2383–2400
- Haggerty R, McKenna SA, Meigs LC (2000) On the late-time behavior of tracer test breakthrough curves. *Water Resources Research* 36(12):3467–3479
- Hayek M, Younes A, Zouali J, et al (2018) Analytical solution and Bayesian inference for interference pumping tests in fractal dual-porosity media. *Computational Geosciences* 22:413–421

- Herrera I, Yates R (1977) Integrodifferential equations for systems of leaky aquifers and applications 3. a numerical method of unlimited applicability. *Water Resources Research* 13(4):725–732
- Hou Z (2003) Mechanical and hydraulic behavior of rock salt in the excavation disturbed zone around underground facilities. *International Journal of Rock Mechanics & Mining Sciences* 40(5):725–738
- Hudson JA, Bäckström A, Rutqvist J, et al (2009) Characterising and modelling the excavation damaged zone in crystalline rock in the context of radioactive waste disposal. *Environmental Geology* 57:1275–1297
- Johansson F, Steinberg V, Kirpichev SB, et al (2017) mpmath: a Python library for arbitrary-precision floating-point arithmetic. <https://doi.org/10.5281/zenodo.1476882>, URL <https://doi.org/10.5281/zenodo.1476882>
- Kazemi H (1969) Pressure transient analysis of naturally fractured reservoirs with uniform fracture distribution. *Society of Petroleum Engineers Journal* 9(04):451–462
- Kim HM, Rutqvist J, Jeong JH, et al (2012) Characterizing excavation damaged zone and stability of pressurized lined rock caverns for underground compressed air energy storage. *Rock Mechanics and Rock Engineering* 46:1113–1124
- Kozeny J (1927) Über kapillare leitung der wasser in boden. *Royal Academy of Science, Vienna, Proc Class I* 136:271–306
- Kranz RL, Frankel AD, Engelder T, et al (1979) The permeability of whole and jointed Barre granite. *International Journal of Rock Mechanics Mineral Sciences and Geomechanical Abstracts* 16:225–234
- Kruseman GP, de Ridder NA (1994) Analysis and evaluation of pumping test data. Tech. Rep. Publication 47, International Institute for Land Reclamation and Improvement, Wageningen, The Netherlands
- Kuhlman KL (2013) Review of inverse Laplace transform algorithms for Laplace-space numerical approaches. *Numerical Algorithms* 63(2):339–355
- Kuhlman KL (2014) Summary results for brine migration modeling performed by LANL, LBNL, and SNL for the UFD program. Tech. Rep. SAND2014–18217R, Sandia National Laboratories, Albuquerque, NM, <https://doi.org/10.2172/1163122>
- Kuhlman KL, Heath JE (2021) Multicontinuum flow models for assessing two-phase flow in containment science. Tech. Rep. SAND2021-7191, Sandia National Laboratories, Albuquerque, NM, <https://doi.org/10.2172/1809129>
- Kuhlman KL, Matteo EN (2018) Porosity and permeability: Literature review and summary. In: *Salt-MechIX*. Federal Institute for Geosciences and Natural Resources (BGR), Hannover, Germany, pp 1–13
- Kuhlman KL, Malama B, Heath JE (2015) Multiporosity flow in fractured low-permeability rocks. *Water Resources Research* 51(2):848–860
- Kuhlman KL, Hardin EL, Rigali MJ (2019) Deep borehole laboratory and borehole testing strategy: Generic drilling and testing plan. Tech. Rep. SAND2019–1896, Sandia National Laboratories, Albuquerque, NM, <https://doi.org/10.2172/1497220>
- Lai CS (1971) Fluid flow through rock salt under various stress states. PhD thesis, Michigan State University, East Lansing, MI
- Le Borgne T, Bour O, De Dreuzy J, et al (2004) Equivalent mean flow models for fractured aquifers: Insights from a pumping tests scaling interpretation. *Water Resources Research* 40(3)

- Lin YC, Yang SY, Fen CS, et al (2016) A general analytical model for pumping tests in radial finite two-zone confined aquifers with Robin-type outer boundary. *Journal of Hydrology* 540:1162–1175
- Liu HH (2014) Non-Darcian flow in low-permeability media: key issues related to geological disposal of high-level nuclear waste in shale formations. *Hydrogeology Journal* 22(7):1525–1534
- Liu HH (2017) *Fluid Flow in the Subsurface*. Springer, New York, NY
- Lommel E (1868) *Studien Über die Bessel'schen Functionen*. von B.G. Teubner
- McLachlan NW (1955) *Bessel Functions for Engineers*, 2nd edn. Oxford
- Mishra PK, Vessilinov V, Gupta H (2013) On simulation and analysis of variable-rate pumping tests. *Groundwater* 51(3):469–473
- Moutsopoulos KN (2021) A simple model for the simulation of the flow behavior in unconfined double porosity aquifers. *Journal of Hydrology* 596(126076)
- Moutsopoulos KN, Papaspyros JN, Fahs M (2022) Approximate solutions for flow in unconfined double porosity aquifers. *Journal of Hydrology* 615(128679)
- Pasandi M, Samani N, Barry DA (2008) Effect of wellbore storage and finite thickness skin on flow to a partially penetrating well in a preatic aquifer. *Advances in Water Resources* 31:383–398
- Perras MA, Diederichs MS (2016) Predicting excvaton damage zone depths in brittle rocks. *Journal of Rock Mechanics and Geotechnical Engineering* 8(1):60–74
- Perras MA, Diederichs MS, Lam T (2010) A review of excavation damage zones in sedimentary rocks with emphasis on numerical modelling for EDZ definition. In: *Proceedings of the 63rd Canadian Geotechnical Conference*, Calgary, Canada, pp 742–750
- Reynolds TD, Gloyne EF (1960) Reactor fuel waste disposal project: Permeability of rock salt and creep of underground salt cavities. Tech. Rep. TID-12383, Atomic Energy Commission Division of Technical Information, Oak Ridge, TN
- Schumer R, Benson DA, Meerschaertm MM, et al (2003) Fractal mobile/immobile solute transport. *Water Resources Research* 39(10):1296
- Shen B, Stephansson O, Rinne M, et al (2011) FRACOD modeling of rock fracturing and permeability change in excavation-damaged zones. *International Journal of Geomechanics* 11(4):302–313
- Spanier J, Oldham KB (1987) *An Atlas of Functions*. Hemisphere
- Stormont JC, Fuenkajorn K (1994) Dilation-induced permeability changes in rock salt. In: *International Conference on Computer Methods and Advances in Geomechanics*, Morgantown, West Virginia, pp 1–5
- Stormont JC, Howard CL, Daemen JJK (1991) Changes in rock salt permeability due to nearby excavation. In: *32nd US Symposium on Rock Mechanics*. OnePetro, Norman, Oklahoma, pp 1–10
- Streltsova TD (1988) *Well Testing in Heterogeneous Formations*. Exxon Monograph, John Wiley & Sons
- Tao J, Shi AC, Li HT, et al (2021) Thermal-mechanical modelling of rock response and damage eveolution during excavation in prestressed goethermal deposits. *International Journal of Rock Mechanics and Mining Sciences* 147:104913
- Theis CV (1935) The relation between the lowering of the piezometric surface and the rate and duration of discharge of a well using ground-water storage. *Transactions, American Geophysical Union* 16:519–524

- Tsang CF, Bernier F, Davies C (2005) Geohydromechanical processes in the excavation damaged zone in crystalline rock, rock salt, and indurated and plastic clays—in the context of radioactive waste disposal. *International Journal of Rock Mechanics and Mining Sciences* 42(1):109–125
- Wallace M, Pietz J, Case J, et al (1990) Coupled fluid-flow modeling of brines flowing through deforming salt around the excavations for the Waste Isolation Pilot Plant (WIPP), in the Permian Salado Formation. In: *Waste Management* 90, Tucson, AZ, pp 1–8
- Wang Y, Zhan H, Huang K, et al (2021) Identification of non-Darcian flow effect in double-porosity fracture aquifer based on multi-well pumping test. *Journal of Hydrology* 600(126541)
- Warren J, Root P (1963) The behavior of naturally fractured reservoirs. *Society of Petroleum Engineers Journal* 3(03):245–255
- Wolfram Research, Inc. (2021) Mathematica, Version 12.3. URL <https://www.wolfram.com/mathematica>, champaign, IL